Heterodyne-detected electronic sum frequency generation: "Up" versus "down" alignment of interfacial molecules

Shoichi Yamaguchi and Tahei Tahara[a)]
Molecular Spectroscopy Laboratory, RIKEN, 2-1 Hirosawa, Wako 351-0198, Japan

(Received 22 July 2008; accepted 21 August 2008; published online 11 September 2008)

Heterodyne-detected electronic sum frequency generation (HD-ESFG) spectroscopy is newly developed to obtain complex electronic $\chi^{(2)}$ spectra of interfaces for a simultaneous detection bandwidth broader than 100 nm. HD-ESFG provides linear $\chi^{(2)}$ spectra that have unambiguous information on the "up" versus "down" alignment of interfacial molecules. It is demonstrated for *p*-nitroaniline, a prototypical molecule of nonlinear optical materials, that the up versus down alignment at an air/fused silica interface is critically influenced by a fine modification of the molecule. © *2008 American Institute of Physics*. [DOI: 10.1063/1.2981179]

Even-order nonlinear optical spectroscopy is a very powerful and unique tool in investigating the structure and dynamics of molecules at interfaces that play key roles in materials and life sciences. The interface selectivity of the even-order nonlinear spectroscopy is based on the principle that $\chi^{(2n)}$ ($2n$ th-order nonlinear optical susceptibility tensor) is zero in the achiral isotropic bulk but can be nonzero at interfaces within the electric dipole approximation.[1] Interface-selective electronic spectra had been obtained by second harmonic generation (SHG),[2] but recently, electronic sum frequency generation (ESFG) was reported by us, which provides a much higher signal to noise ratio with much shorter measurement time by virtue of the multiplex advantage.[3–6]

ESFG and SHG measurements provide data representing $|\chi^{(2)}|^2$, not $\chi^{(2)}$ itself, because of the homodyne nature of signal detection. This feature sometimes makes interpretation of data difficult, and even worse, it hides essential information inherent in $\chi^{(2)}$. The most crucial information lost in the homodyne detection is the sign of $\chi^{(2)}$ that is directly related to the "up" versus "down" alignment of interfacial molecules.[1]

The interfacial molecular alignment primarily influences and/or reflects interfacial properties such as hydrophobicity and hydrophilicity, surface potential, and surface tension. Therefore, numbers of heterodyne-detection experiments have been performed to determine the sign of interfacial $\chi^{(2)}$. The phase-sensitive SHG method developed by Chang *et al.*[7] was first applied to a liquid interface by Kemnitz *et al.*,[8] and later it was followed by many groups.[9] Interferometric SHG in the frequency domain was demonstrated by Wilson *et al.*[10] who determined complex $\chi^{(2)}$ phases of solid interfaces for the bandwidth of 20 nm. The same technique was reported also by Veenstra *et al.*[11] independently. Phase-sensitive measurements of IR-visible vibrational sum frequency generation (VSFG) have been performed first by Shen and co-workers,[12,13] and recently, multiplex heterodyne-detected VSFG was demonstrated by Stiopkin *et al.*[14] In the present Communication, we report on the development of heterodyne-detected ESFG (HD-ESFG) that provides complex electronic $\chi^{(2)}$ spectra for a bandwidth of more than 100 nm, and its application to unambiguous determination of the up versus down alignments of *p*-nitroaniline (PNA) and its derivative *N*,*N*′-diethyl-*p*-nitroaniline (DEPNA) adsorbed at a glass surface.

Figure 1(a) shows the schematic of the experimental setup for HD-ESFG. Narrow-band ω_1 (795 nm) and broadband ω_2 (540 nm–1.2 μm) pulses are noncollinearly focused onto the same spot at the interface of a sample. The linear polarization of the ω_1 and ω_2 pulses is in the plane of reflection (i.e., *p* polarization). When the ω_1 and ω_2 pulses are temporally overlapped, the sum frequency ($\omega_1+\omega_2$) is generated at the interface. In original homodyne-detected ESFG, the spectrum of this sum frequency light was directly detected.[3–6] In HD-ESFG, however, the ω_1, ω_2, and $\omega_1+\omega_2$ pulses are again focused by a spherical concave mirror onto a GaAs(110) surface to generate the sum frequency of ω_1 and ω_2 once more. A fused silica glass plate with a 1 mm thickness is placed between the sample and the concave mirror. The glass substrate delays the $\omega_1+\omega_2$ pulse relative to the reflected ω_1 pulse by 170 fs due to frequency dependent differences in the group velocity. This delay results in the time difference between the $\omega_1+\omega_2$ pulse generated from the sample and that from GaAs. (Note that the difference in the group velocities at ω_2 and ω_1 is so small that their temporal overlap at the GaAs surface is held.) The $\omega_1+\omega_2$ pulse from the sample and that from GaAs propagate collinearly and sequentially through an analyzer, selecting the *p* polarization, and enter into a polychromator. After spectrally dispersed, the $\omega_1+\omega_2$ sum frequency light is detected by a multichannel detector.

Figure 1(b) shows a raw spectrum obtained in the HD-ESFG measurement for a submonolayer film of PNA spin coated on a fused silica glass substrate. In sharp contrast to homodyne-detected ESFG spectra,[3,4,6] fine fringes are superimposed in the present spectrum. These fringes are due to the interference between the sum frequency light from the sample and that from GaAs. Information on the complex

[a)]Electronic mail: tahei@riken.jp.

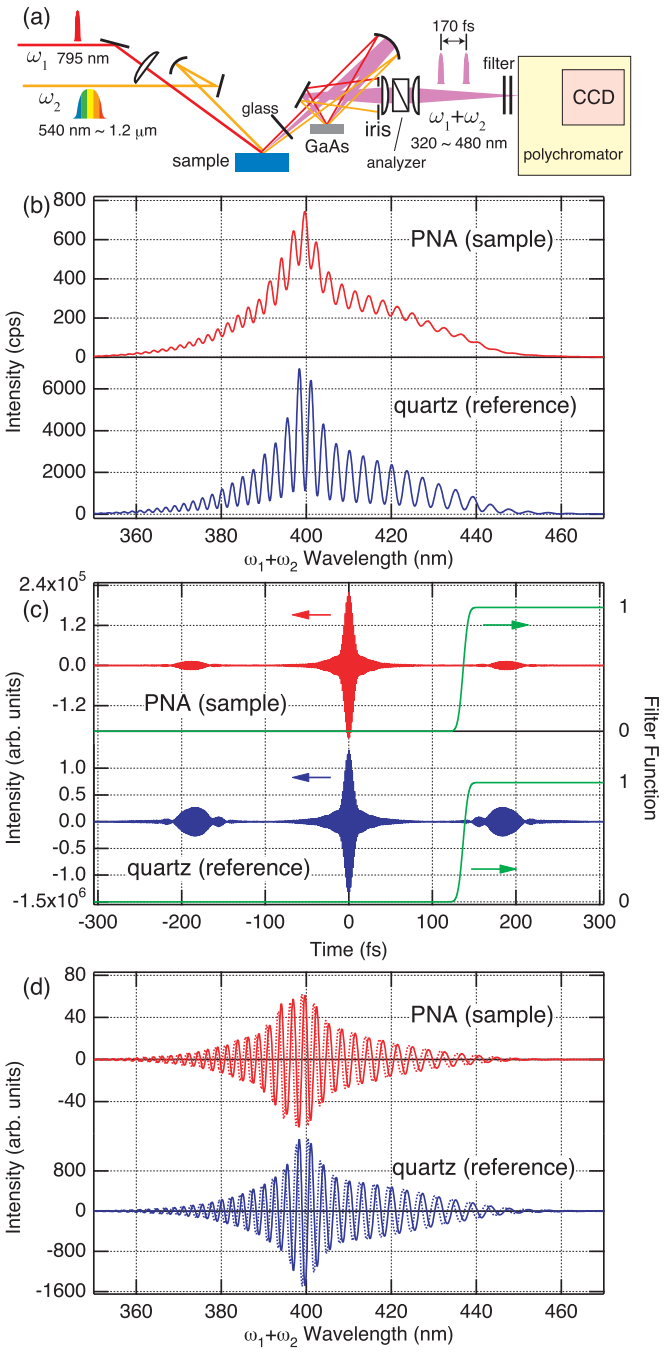

FIG. 1. (Color) (a) Schematic of the HD-ESFG experimental setup. (b) Raw $|\tilde{E}_{\text{total}}|^2$ spectra of PNA at the air/fused silica interface (red line) and the left-handed y-cut quartz crystal (blue line). (c) Time-domain interferograms obtained by the inverse Fourier transformation of the $|\tilde{E}_{\text{total}}|^2$ spectra of PNA (red line) and the quartz (blue line). The interferograms look painted red or blue because of very fine fringes. Because the real and imaginary parts of the interferograms have the same envelope, only the real parts are shown here. The filter function (green line) is plotted to the right vertical axis. (d) $\tilde{E}_{\text{sample}}\tilde{E}^*_{\text{GaAs}}\exp(i\omega T)$ spectrum of PNA (red lines) obtained by the Fourier transformation of the time-domain interferogram after the filtration and $\tilde{E}_{\text{quartz}}\tilde{E}'^*_{\text{GaAs}}\exp(i\omega T)$ spectrum of the quartz (blue lines) obtained in the same way. The solid and dotted lines represent the real and imaginary parts, respectively.

phase of $\chi^{(2)}$ of PNA is contained in the interference fringes. In Fig. 1(b), a raw spectrum of the y-cut surface of a left-handed quartz crystal is also shown. The quartz is set at the same position as the PNA sample. The spectrum of the quartz exhibits larger fringes than that of PNA, reflecting the larger $|\chi^{(2)}|$ of the quartz surface. This spectrum of the quartz is used as a reference.

The total electric field of the sum frequency light $E_{\text{total}}(t)$ is expressed in the time domain as follows:

$$E_{\text{total}}(t) = E_{\text{sample}}(t-T) + E_{\text{GaAs}}(t), \tag{1}$$

where $E_{\text{sample}}(t)$ and $E_{\text{GaAs}}(t)$ are the electric field of the sum frequency light from the sample and that from GaAs, respectively, and T is the time delay between them. In the present experiment, T is equal to 170 fs. Equation (1) is Fourier transformed into the frequency domain in the following way:

$$\tilde{E}_{\text{total}}(\omega) = \int_{-\infty}^{\infty} dt E_{\text{total}}(t)\exp(i\omega t)$$

$$= \tilde{E}_{\text{sample}}(\omega)\exp(i\omega T) + \tilde{E}_{\text{GaAs}}(\omega), \tag{2}$$

where the tilde indicates the electric field in the frequency domain. The raw spectrum shown in Fig. 1(b) corresponds to the absolute square of the total electric field of Eq. (2), which can be expressed as follows:

$$|\tilde{E}_{\text{total}}|^2 = |\tilde{E}_{\text{sample}}|^2 + |\tilde{E}_{\text{GaAs}}|^2 + \tilde{E}_{\text{sample}}\tilde{E}^*_{\text{GaAs}}\exp(i\omega T)$$

$$+ \tilde{E}^*_{\text{sample}}\tilde{E}_{\text{GaAs}}\exp(-i\omega T). \tag{3}$$

The third and fourth terms of the right-hand side (rhs) of Eq. (3) are the origin of the interference fringes in the raw $|\tilde{E}_{\text{total}}|^2$ spectrum in Fig. 1(b). The inverse Fourier transformation of the $|\tilde{E}_{\text{total}}|^2$ spectrum gives the time-domain interferogram shown in Fig. 1(c), where the third and fourth terms of the rhs of Eq. (3) give the peaks at $t=+T(=+170$ fs) and $-T(=-170$ fs), respectively. The peak at $t=0$ fs is ascribed to the first and second terms of the rhs of Eq. (3). Because the peaks in the time-domain interferogram are well separated, the peak at $t=+T$ can be readily extracted by multiplying the interferogram by a filter function depicted in Fig. 1(c). This filtering of the time-domain interferogram followed by the Fourier transformation back into the frequency domain gives the complex spectrum of the third term, $\tilde{E}_{\text{sample}}\tilde{E}^*_{\text{GaAs}}\exp(i\omega T)$, which is shown in Fig. 1(d).

The sum frequency electric fields $\tilde{E}_{sample}$ and $\tilde{E}_{\text{GaAs}}$ are expressed by using the second-order nonlinear susceptibilities of the sample and GaAs ($\chi^{(2)}_{\text{sample}}$, $\chi^{(2)}_{\text{GaAs}}$) as well as the electric fields of the ω_1 and ω_2 pulses ($\tilde{E}_1$, $\tilde{E}_2$):

$$\tilde{E}_{\text{sample}} = ia_{\text{sample}}\chi^{(2)}_{\text{sample}}\tilde{E}_1\tilde{E}_2, \tag{4}$$

$$\tilde{E}_{\text{GaAs}} = a_{\text{GaAs}}\chi^{(2)}_{\text{GaAs}}r_1^{sample}\tilde{E}_1 r_2^{sample}\tilde{E}_2, \tag{5}$$

where a_{sample} and a_{GaAs} are real and positive constants[1,2,15] and r_1^{sample} and r_2^{sample} are the reflectivities of the sample for $\tilde{E}_1$ and $\tilde{E}_2$, respectively. (Because the bulk of the sample is not $\chi^{(2)}$ active, the rhs of Eq. (4) contains i.[1] In Eq. (5), the rhs does not contain i because the bulk of GaAs is $\chi^{(2)}$ active.[2,15,16]) As understood by Eqs. (4) and (5), $\tilde{E}_{\text{sample}}\tilde{E}^*_{\text{GaAs}}\exp(i\omega T)$ is proportional to $\chi^{(2)}_{\text{sample}}$.

The $\chi^{(2)}_{\text{sample}}$ spectrum can be obtained by canceling out $\tilde{E}_1$, $\tilde{E}_2$, and $\chi^{(2)}_{\text{GaAs}}$ in $\tilde{E}_{\text{sample}}\tilde{E}^*_{\text{GaAs}}\exp(i\omega T)$, which is realized

by normalization with a reference spectrum. Figure 1(d) shows the reference spectrum $\tilde{E}_{\text{quartz}}\tilde{E}'^{*}_{\text{GaAs}}\exp(i\omega T)$ acquired from the raw $|\tilde{E}_{\text{total}}|^2$ spectrum of the left-handed y-cut quartz crystal [Fig. 1(b)]. [The time-domain interferogram of the quartz is also shown in Fig. 1(c).] The sum frequency electric fields $\tilde{E}_{\text{quartz}}$ and $\tilde{E}'^{*}_{\text{GaAs}}$ are expressed as follows:

$$\tilde{E}_{\text{quartz}} = a_{\text{quartz}}\chi^{(2)}_{\text{quartz}}\tilde{E}_1\tilde{E}_2, \tag{6}$$

$$\tilde{E}'_{\text{GaAs}} = a_{\text{GaAs}}\chi^{(2)}_{\text{GaAs}}r_1^{\text{quartz}}\tilde{E}_1 r_2^{\text{quartz}}\tilde{E}_2, \tag{7}$$

where $\chi^{(2)}_{\text{quartz}}$ is $\chi^{(2)}$ of the quartz, a_{quartz} is a real and positive constant,[2,15] and r_1^{quartz} and r_2^{quartz} are the reflectivities of the quartz for $\tilde{E}_1$ and $\tilde{E}_2$, respectively. [Because the bulk of the quartz is $\chi^{(2)}$ active, the rhs of Eq. (6) does not contain i.[2,15]] $\chi^{(2)}_{\text{quartz}}$ can be regarded as a real constant because of the absence of electronic resonances for the quartz in the ω_1, ω_2, and $\omega_1+\omega_2$ energy regions. Using Eqs. (4)–(7), we obtain the following formula:

$$\frac{\tilde{E}_{\text{sample}}\tilde{E}^{*}_{\text{GaAs}}\exp(i\omega T)}{i\tilde{E}_{\text{quartz}}\tilde{E}'^{*}_{\text{GaAs}}\exp(i\omega T)} = \frac{a_{\text{sample}}r_1^{\text{sample}}r_2^{\text{sample}}}{a_{\text{quartz}}r_1^{\text{quartz}}r_2^{\text{quartz}}\chi^{(2)}_{\text{quartz}}}\chi^{(2)}_{\text{sample}}. \tag{8}$$

This formula means that the spectrum of $\chi^{(2)}_{\text{sample}}$ can be obtained by normalizing the $\tilde{E}_{\text{sample}}\tilde{E}^{*}_{\text{GaAs}}\exp(i\omega T)$ spectrum [Fig. 1(d), red lines] by the $\tilde{E}_{\text{quartz}}\tilde{E}'^{*}_{\text{GaAs}}\exp(i\omega T)$ spectrum [Fig. 1(d), blue lines] with i because the product of all the coefficients preceding $\chi^{(2)}_{\text{sample}}$ in the rhs of Eq. (8) is real and positive. (Note that the positive x axis of the left-handed y-cut quartz was directed to the propagation direction of the light in the experiment to set $\chi^{(2)}_{\text{quartz}}$ positive.[8,17])

Figure 2(a) shows the complex $\chi^{(2)}$ spectrum of PNA ($\chi^{(2)}_{\text{PNA}}$) at the air/fused silica interface obtained by the normalization. The real part of $\chi^{(2)}_{\text{PNA}}$ has a dispersive feature, and the imaginary part exhibits a symmetric band shape. This real-imaginary relation is consistent with the resonance condition of the present experiment: PNA has an electronic structure that is only two-photon ($\omega_1+\omega_2$) single resonant. ("Two-photon single resonant" means that the $\omega_1+\omega_2$ pulse is in resonance with an excited state, but the ω_1 and ω_2 pulses are not in resonance.) Actually, if the homogeneous broadening and the Lorentz function is assumed for the electronic transition of PNA, the real and imaginary parts of $\chi^{(2)}_{\text{PNA}}$ show the dispersive and symmetric features, respectively. The electronic resonance in the $\chi^{(2)}_{\text{PNA}}$ spectrum is assigned to the transition from the ground state to the lowest singlet state that is one- and two-photon allowed.

We also performed HD-ESFG measurements for DEPNA in which the amino group of PNA is replaced with the diethylamino group. Figure 2(b) shows the complex $\chi^{(2)}$ spectrum of submonolayer DEPNA at the air/fused silica interface ($\chi^{(2)}_{\text{DEPNA}}$) which was prepared in the same way as PNA. Apart from the shift in the peak wavelength of the electronic resonance, the most remarkable difference between the $\chi^{(2)}_{\text{PNA}}$ and $\chi^{(2)}_{\text{DEPNA}}$ spectra is the sign. Clearly, the real and imaginary parts of $\chi^{(2)}_{\text{DEPNA}}$ exhibit the opposite signs

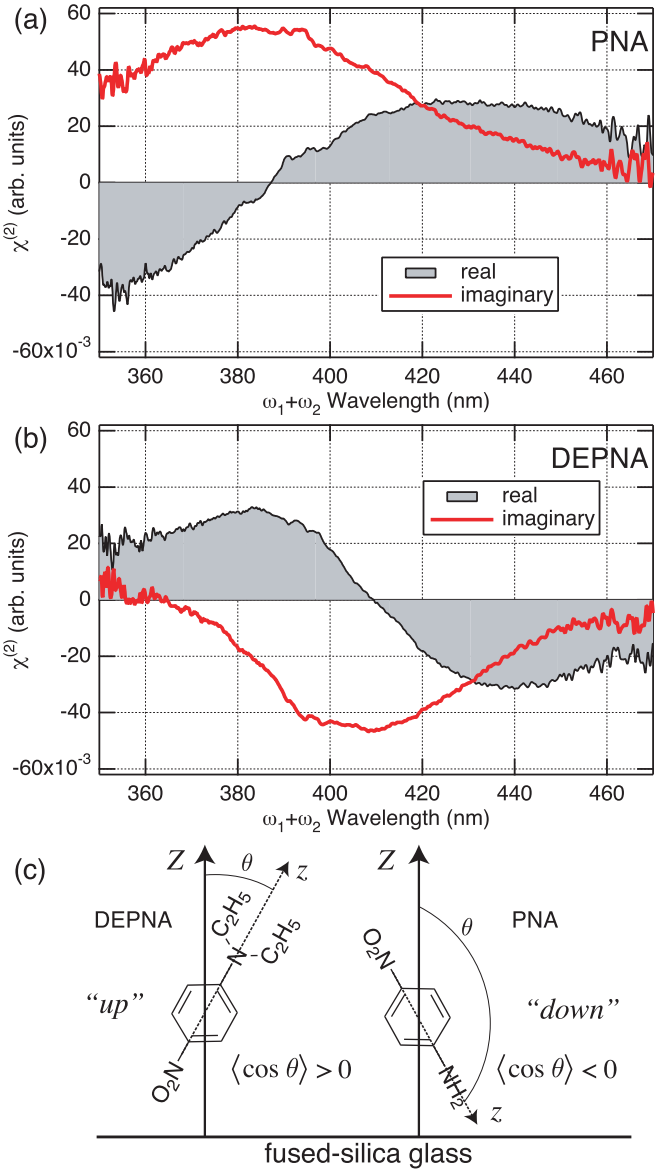

FIG. 2. (Color) [(a) and (b)] Complex $\chi^{(2)}$ spectra of PNA (a) and DEPNA (b) at the air/fused silica interface. The black and red lines represent the real and imaginary parts, respectively. (c) Schematic of the up and down alignments of DEPNA and PNA at the air/fused silica interface.

to those of $\chi^{(2)}_{\text{PNA}}$, which is attributable to the change in the up versus down alignment between PNA and DEPNA.

$\chi^{(2)}_{\text{PNA}}$ and $\chi^{(2)}_{\text{DEPNA}}$ obtained in the HD-ESFG measurements correspond to the so-called $\chi^{(2)}_{ppp}$ that stands for $\chi^{(2)}$ measured with all the input and output beams p-polarized. $\chi^{(2)}_{ppp}$ can be expressed with the molecular hyperpolarizability tensor $\beta^{(2)}$ and the molecular tilt angle θ [between the interface-normal Z axis and the molecular z axis, schematically shown in Fig. 2(c)] in the following way:[1,18,19]

$$\chi^{(2)}_{ppp} = a\left(\frac{\langle\cos^3\theta\rangle}{\langle\cos\theta\rangle} - b\right)\langle\cos\theta\rangle\beta^{(2)}_{zzz}, \tag{9}$$

where the parameters a and b are real and positive and the brackets mean the ensemble average of the orientational distribution at the interface. Quantum chemical calculations showed that $\beta^{(2)}_{zzz}$ in resonance with the lowest one- and two-photon allowed singlet state has a positive imaginary part

and a positively dispersive real part for PNA and DEPNA when the z-axis direction is defined from the nitro group to the amino or diethylamino group.[20–22] Therefore, the positive imaginary $\chi^{(2)}_{\mathrm{PNA}}$ spectrum in Fig. 2(a) indicates that $\chi^{(2)}_{ppp}/\beta^{(2)}_{zzz}$ is positive for PNA, whereas the negative imaginary $\chi^{(2)}_{\mathrm{DEPNA}}$ spectrum in Fig. 2(b) implies that $\chi^{(2)}_{ppp}/\beta^{(2)}_{zzz}$ is negative for DEPNA. We performed polarization SHG measurements and found that $\langle\cos^3\theta\rangle/\langle\cos\theta\rangle - b$ is negative for the PNA and DEPNA samples.[23] Therefore, it is straightforwardly concluded that $\langle\cos\theta\rangle$ is negative (i.e., down alignment) for PNA and positive (i.e., up alignment) for DEPNA.

The absolute orientations of the two molecules at the air/fused silica interface are illustrated in Fig. 2(c). DEPNA takes the up alignment: The diethylamino group points upward to the air and the nitro group points downward to the fused silica. This alignment fits our intuition that the nonpolar diethylamino group points to the "nonpolar" air side and the polar nitro group points to the "polar" fused silica side. In fact, the fused silica surface is known to provide a polar environment, and consistently, the imaginary $\chi^{(2)}_{\mathrm{DEPNA}}$ and $\chi^{(2)}_{\mathrm{PNA}}$ spectra in Fig. 2 are located at similar wavelengths to the UV-visible absorption spectra of PNA and DEPNA in polar solvents.[24,25] The alignment of PNA is opposite to that of DEPNA: the amino group points downward to the fused silica and the nitro group points upward to the air. Although both of the two end groups of PNA are polar, the hydrogen-bonding interaction between the amino group and the surface OH group of the fused silica is so strong that it makes the alignment down, which is reasonable from the viewpoint of interfacial chemistry.[26] PNA and DEPNA are similar molecules, but the modification of the amino group brings about the opposite alignments on the fused silica surface.

ACKNOWLEDGMENTS

This work was supported by a Grant-in-Aid for Scientific Research on Priority Area "Molecular Science for Supra Functional Systems" (Grant No. 19056009) from MEXT and a Grant-in-Aid for Scientific Research (A) (Grant No. 19205005) from JSPS. We thank the RIKEN Super Combined Cluster (RSCC) for the computational resources.

[1] T. F. Heinz, in *Nonlinear Surface Electromagnetic Phenomena*, edited by H.-E. Ponath and G. I. Stegeman (Elsevier, Amsterdam, 1991), Vol. 29, p. 353.
[2] Y. R. Shen, *The Principles of Nonlinear Optics* (Wiley, New York, 1984).
[3] S. Yamaguchi and T. Tahara, J. Phys. Chem. B **108**, 19079 (2004).
[4] S. Yamaguchi and T. Tahara, J. Chem. Phys. **125**, 194711 (2006).
[5] K. Sekiguchi, S. Yamaguchi, and T. Tahara, J. Chem. Phys. **128**, 114715 (2008).
[6] S. Yamaguchi and T. Tahara, Laser Photonics Rev. **2**, 74 (2008).
[7] R. K. Chang, J. Ducuing, and N. Bloembergen, Phys. Rev. Lett. **15**, 6 (1965).
[8] K. Kemnitz, K. Bhattacharyya, J. M. Hicks, G. R. Pinto, K. B. Eisenthal, and T. F. Heinz, Chem. Phys. Lett. **131**, 285 (1986).
[9] R. Lü, Y. Rao, W. Zhang, and H. Wang, SPIE Conference on Nonlinear Spectroscopy, Seattle, WA, 2002 (unpublished), Vol. 4812, p. 115, and references therein.
[10] P. T. Wilson, Y. Jiang, O. A. Aktsipetrov, E. D. Mishina, and M. C. Downer, Opt. Lett. **24**, 496 (1999).
[11] K. J. Veenstra, A. V. Petukhov, A. P. d. Boer, and T. Rasing, Phys. Rev. B **58**, R16020 (1998).
[12] R. Superfine, J. Y. Huang, and Y. R. Shen, Opt. Lett. **15**, 1276 (1990).
[13] V. Ostroverkhov, G. A. Waychunas, and Y. R. Shen, Chem. Phys. Lett. **386**, 144 (2004).
[14] I. V. Stiopkin, H. D. Jayathilake, A. N. Bordenyuk, and A. V. Benderskii, J. Am. Chem. Soc. **130**, 2271 (2008).
[15] N. Bloembergen and P. S. Pershan, Phys. Rev. **128**, 606 (1962).
[16] If the surface $\chi^{(2)}$ of GaAs in the present in-plane orientation is not negligible compared with the bulk $\chi^{(2)}$, it is necessary to regard a_{GaAs} as complex. However, this point will not affect the $\chi^{(2)}$ spectra in Fig. 2 because a_{GaAs} is canceled out in the normalization.
[17] X. Wei, S. C. Hong, X. Zhuang, T. Goto, and Y. R. Shen, Phys. Rev. E **62**, 5160 (2000).
[18] G. L. Richmond, Chem. Rev. (Washington, D.C.) **102**, 2693 (2002).
[19] W. Zhang, H. Wang, and D. Zheng, Phys. Chem. Chem. Phys. **8**, 4041 (2006).
[20] S. J. Lalama and A. F. Garito, Phys. Rev. A **20**, 1179 (1979).
[21] S. P. Karna and P. N. Prasad, J. Chem. Phys. **94**, 1171 (1991).
[22] We performed time-dependent density functional theory calculations and found that the imaginary part of $\beta^{(2)}_{zzz}$ (in resonance with the lowest allowed state) is positive for PNA and DEPNA. Our calculation results are consistent with Refs. 20 and 21 as regards PNA.
[23] The polarization SHG measurements showed that $\langle\cos^3\theta\rangle/\langle\cos\theta\rangle = 0.58$ and $b=0.66$ for PNA and $\langle\cos^3\theta\rangle/\langle\cos\theta\rangle = 0.56$ and $b=0.61$ for DEPNA. If the δ function is assumed for the orientational distribution (i.e., $\langle\cos^3\theta\rangle/\langle\cos\theta\rangle = \cos^2\theta$), $\theta=140°$ for PNA and $\theta=42°$ for DEPNA.
[24] H. Wang, E. Borguet, and K. B. Eisenthal, J. Phys. Chem. A **101**, 713 (1997).
[25] M. J. Kamlet, R. R. Minesinger, E. G. Kayser, M. H. Aldridge, and J. W. Eastes, J. Org. Chem. **36**, 3852 (1971).
[26] G. S. Caravajal, D. E. Leyden, G. R. Quinting, and G. E. Maciel, Anal. Chem. **60**, 1776 (1988).